Aerodynamic Optimization of a High-speed Train using Genetic Algorithms

J.Muñoz-Paniagua, J. García, A. Crespo

Department of the Energy and Applied Fluid Mechanics, Universidad Politécnica de Madrid
C/José Gutiérrez Abascal 2, 28006, Madrid, Spain

le.munoz@upm.es.

Abstract

Genetic algorithms (GA) have been used for the minimization of the aerodynamic drag of a train subject to front wind. The significant importance of the external aerodynamic drag on the total resistance a train experiments as the cruise speed is increased highlights the interest of this study. A complete description of the methodology required for this optimization method is introduced here, where the parameterization of the geometry to be optimized and the metamodel used to speed up the optimization process are detailed. A reduction of about a 25% of the initial aerodynamic drag is obtained in this study, what confirms GA as a proper method for this optimization problem. The evolution of the nose shape is consistent with the literature.The advantage of using metamodels is stressed thanks to the information of the whole design space extracted from it. The influence of each design variable on the objective function is analyzed by means of an ANOVA test.

INTRODUCTION

Even when the train makes the most economical use of energy form of public transport, reducing energy consumption is claimed. One contributor to the consumption of the energy put into a high-speed train (HST) is the aerodynamic drag, which takes a more relevant role as the cruise speed is increased. Therefore, the interest in the aerodynamic drag of HST has grown considerably during the last decades, with a view to reducing energy consumption. The aerodynamic drag of HST has been object of study in [1] and [2] for zero-yaw-angle or front wind conditions. [3-5] estimate the contribution of different constructive elements of a HST to the total aerodynamic drag. Regional trains have been studied by [6], while freight trains have been investigated in [7]. The optimization of the nose shape to reduce the aerodynamic drag has been developed for HST in [8-9] in front wind conditions, at the entrance of a tunnel in [10] while in [11] the addition of flow control devices is adopted for decreasing the pressure drag on an ICE 2 train model.

Although it is evident the correlation between the energy consumption and the train aerodynamic drag, the fact that streamlined nose designs are considered for HST makes this aerodynamic issue not the most demanding one. Indeed, other problems like cross-wind stability or aerodynamics in tunnel result into more complex situations that have been object of many investigations. These aerodynamic objectives are left for study in further investigations. Nevertheless, the simplicity of the simulations in front wind conditions results into an advantage for the set-up of the new optimization approach introduced in this paper, and so this problem is the one to be faced here. The objective of this chapter is the optimization of the train nose (and tail) shape under zero cross-wind in order to minimize the aerodynamic drag on the train. Such optimization is performed using genetic algorithms as the optimization method. The estimation of the aerodynamic drag on a train serves as a theoretical introduction for this paper. After that, a brief description of the genetic algorithm method is presented, including the methodology related to the performance of this method. The geometry to be optimized and the metamodel to be used are introduced. A discussion of the main results of the aerodynamic optimization receive major attention of the paper. Finally, last section is devoted to the summary and conclusions.

PHENOMENA DESCRIPTION

In general, a desirable train system should be aerodynamically stable and have low aerodynamic forces. These forces are obviously influenced by the particular features in the aerodynamics of the HST. Different expressions are available since time ago to estimate the total resistance a train experiences when traveling in open air.

Among them, the most accepted one is Davis formula, from 1926, [4],

$$R = A + (B_1 + B_2)U_\infty + CU_\infty{}^2, \tag{1}$$

where U_∞ is the train speed relative to the air (assumed to be the same as the relative one to the ground (original formula considers possible difference between train speed relative to the ground (acting on B_1) and train speed relative to the air (affecting B_2 and C)). The total resistance R is divided into mechanical and external aerodynamic resistance. The coefficient A is the rolling mechanical resistance, B_1 makes reference to transmission losses and brake drag, and B_2 is air momentum drag associated with the energy required to generate the internal flow need for engine cooling or air conditioning, [4]. External aerodynamic drag is expressed by C. Values of these coefficients are obtained experimentally. It is observed that mechanical drag is proportional to speed while aerodynamic one is proportional to the square of speed. Thus, it is evident the vital importance of reducing the aerodynamic drag when HST are considered. For streamlined trains at speeds around 300 km h^{-1}, 80% of the total resistance is caused by external aerodynamic drag, [4].

The aerodynamic drag D results in the sum of two contributions, the pressure drag and the friction drag.

$$D = CU_\infty{}^2 = \frac{1}{2}\rho A U_\infty{}^2 \left(C_{Dp} + \frac{\lambda}{d} L \right), \tag{2}$$

with ρ the density of air, A the frontal area of train, C_{Dp} the pressure drag coefficient, d and L the train hydraulic diameter and length respectively, and λ the train friction coefficient. Pressure drag is not dependent on the train length. However, friction drag does, as it includes drags related to pantographs, inter-car gaps or underbody elements. The pressure drag is caused by the fore- and after-bodies of train. Different studies point out that there is no significant difference in drag produced by a large variety of slender shapes if sharp edges are avoided, [4]. The effects of the nose (and tail) shape on the overall drag of a train are quite small, about a 10%, compared to about a 30% of the external aerodynamic drag that is caused by skin friction, [4], which can increase to a 90% for very large trains (16 coaches), [3]. Baker [1] points out that, in conditions of zero cross-wind, the variations of air velocity and pressure in the nose region are essentially inviscid, and Schetz [4] indicates that the drag caused by the nose and tail are governed more by the underbelly flow than by the flow over the exposed surfaces. Indeed, it is the underneath structures of train that has a larger contribution to the total aerodynamic drag (about 50%). However, it is still possible to obtain appreciable variations of the drag changing the train nose and tail shape, [3], where differences of the aerodynamic drag of about a 33% were observed for a large set of train nose shapes. Geometric modifications of the nose shape were considered as well in [8] for the aerodynamic optimization of the EMUV250 train model, and Orellano [9] observed differences of the aerodynamic drag of about 25% from best-to-worst train nose design included in his study. Consequently, these references lead us to think that there is potential to aerodynamically optimize the nose of a HST even if only this region of the train is under consideration.

METHODOLOGY

The optimization method used here for the minimization of the aerodynamic drag of a HST in zero cross-wind situation is the genetic algorithm (GA). GA, introduced by Holland [12] and developed by Goldberg, [13], are a technique that mimic the mechanics of the natural evolution. Once a population of potential solutions is defined, three operators (selection of the fittest, reproduction or crossover and mutation) are applied, Fig (1). Iteratively, a new population is generated and better results are obtained until a solution closer to globally optimal solution is reached. The combination of the survival-of-the-fittest concept to eliminate unfit characteristics with a random information exchange and the exploitation of the knowledge contained in old solutions permit GA to effect a search mechanism with efficiency and speed. GA are englobed in zero-order methods, based on direct evaluations of the objective function. This is an advantage compared to first-order methods that need the calculation of the first derivative of the objective function. However, the large number of evaluations required when using GA is a disadvantage that minimizes its power, moreover when compared to the adjoint method [14]. Nevertheless, the simplicity and robustness of this optimization method put the GA into a prevailing position, specially for this problem where the nature of the flow is not so complex.

To minimize the problem of the large number of evaluations required by the GA, which directly depends on the dimensionality of the design space, a simple, while at the same time precise, geometrical parameterization was proposed. Additionally, the CFD solver call was substituted by a metamodel. The present increase of the

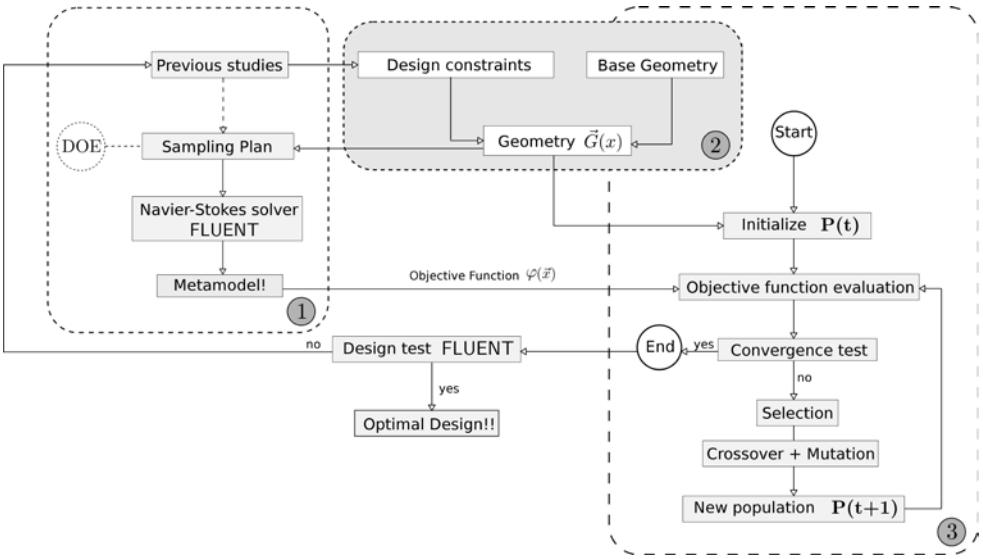

Fig. 1. Schematic representation of the whole optimization method.

computational power is not sufficient to conceive a thorough search of the design space using accurate simulations. This situation leads to the introduction of an approximate model whose computational cost is much lower than the relative to the CFD simulation. In Fig. (1), a very conventional optimization work-flow is represented. This scheme refers to an online optimization, where after the end of the GA optimization process, the best solution found by the surrogate-based optimizer is evaluated and verified, and this new simulation is added to the initial database that was used to train or fit the coefficients of the metamodel.

The methodology considered to optimize the high-speed nose using the GA is represented in Fig. (1). In this figure three blocks are depicted, referred to the main steps in the optimization process when using GA. Blocks #1 and #2 are related to the pre-optimization issues, namely the shape parameterization and the construction of the metamodel or surrogate-model. The geometry is parameterized using Bèzier curves as it will be explained afterwards, and a set of points that trace the curves for the definition of the train nose volume is created. MATLAB is used for the implementation of the Bèzier curves and for exporting this set of auxiliary points. This information is later imported in CATIA, where the train nose and the train body are created. Once the geometry is created, it is collected within the sampling plan that define the design of experiments (DoE). All the geometries are evaluated using a Navier-Stokes solver (ANSYS-FLUENT), and this information is used to train and fit the metamodel. The metamodel is generated using MINAMO, where functions already implemented in the software are used to construct it. The training of the metamodel is the final step of the pre-optimization. When the metamodel is set, the optimization process starts itself. The GA is already coded in MINAMO, so it is not necessary to program all the operators and functions of the GA. The optimization continues until convergence is achieved. The optimal design obtained in the optimization process needs to be validated using a more accurate evaluation (*i.e.* a simulation in ANSYS-FLUENT), and if the result is not satisfactory (because the quality of the metamodel is not yet enough or because the optimal candidate is not the best one), the pre-optimization process has to be re-started. This is known as online optimization. As it can be observed, different programs are required to complete the optimization process, and when online optimization' is considered, several iterations are necessary. To control all this software calls and to automate this optimization process in a smart way, MINAMO was used. In summary, four commercial software were required for the whole optimization process.

GEOMETRIC PARAMETERIZATION

By means of a certain number of design variables, shape parameterization provides a representation of the design space, defining the shape of any geometry. Thus, a complete, simple and precise selection of these design variables (and its range of variation) is critical for the parameterization effectiveness. Different shape parameterization techniques are available, among which Bèzier curves are selected. Bèzier curves are highly suited for shape optimization, as they can describe a curve in a very compact form with a small set of design variables. The equation of the curve is

$$\mathbf{C}(\mathrm{t}) = \sum_{i=0}^{n} \binom{n}{i} (1-t)^{n-i} t^{i} \mathbf{P}_{\mathrm{i}} \tag{3}$$

where $0 \leq t \leq 1$ is a parameter control, and $\mathbf{P}_{\mathrm{i}}$ are the control points that define the curve. The first and last control points are always the end points of the curve, however the intermediate control points (if any) generally do not lie on the curve. The characteristics of the curve are strongly coupled with the underlying polygon of these control points, simplifying the link between parameters and real design variables. The parameterization is reduced to the definition of the coordinates of these control points.

Once the parameterization technique is selected, and before a review of the most relevant conclusions from previous works is carried out, it is necessary to chose a reference geometry. We have chosen a smooth model of the leading control unit of the Inter-City Express (ICE) 2 train. This is known as the Aerodynamic Train Model (ATM), which is widely accepted among the train aerodynamics community as a reference geometry. No details of pantograph, bogies, partial bogies skirts, plough underneath the front-end or inter-car gap are included.

As HST are designed to be bidirectional, with identical leading and trailing cars, so the nose and tail shape are assumed to be the same , the application of the GA and the parameterization is restricted only to the ends of the train. This means that the geometry to be parameterized is the nose and tail. Since all the optimal candidates will be attached to the same train coach, the cross-section of the train is constant for all the geometries. Thus, the cross-section is obtained by sampling the actual cross-section of the ATM train model. Its height H_t and width b_t are considered as reference lengths for the following geometry definition. From [3], maximum nose length where to observe notable changes in drag coefficient when front wind is affecting the train is two times the train width. Therefore, the length of the train head L_t is already fixed. The values of these constant parameters, apart from other significant contants, are given in Table (1).

Table 1. Geometric constants obtained from ATM. All the lengths are given in mm.

H_t	3891.3	b_t	3036.0	L_t	6000.0	H_{bajos}	261.0	$l_{deflector}$	1258.1

Following Rho proposal, the nose (and tail) of the train is divided into four section-boxes, namely the roof, windshield, hood and underbody section, so that for the lateral view, four Bèzier curves are used for the description of the nose shape. The underbody is supposed as horizontal. The three-dimensional (3D) shape is obtained with six extra curves (thanks to the longitudinal symmetry of the train). More information about the parameterization of the geometry can be found in [16]. To illustrate the resulting parametric description of the nose, in Fig. (2) it is represented the Bèzier curve that defines the windshield shape in the symmetry plane (*xz*). The coordinates of the control points of this curve are given in Table (2). A total number of 25 design variables are used for the whole description of the nose of the ATM. The range of variation of these is indicated in Table (3).

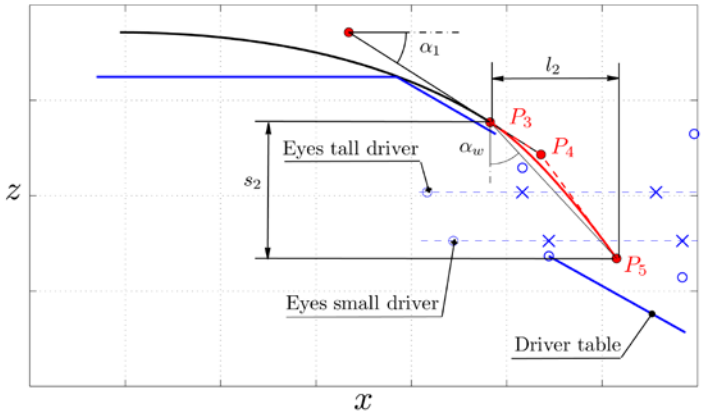

Fig. 2. Windshield parameterization in the longitudinal symmetry plane (xz). The red line represents the windshield given by a quadratic Bèzier curve. The red dots refer to the control points. The dashed red line represents the control polygon. In blue, the geometry restrictions of the driver cabin size and driver table are given. It is also indicated the position of the eyes of a 'tall' and a 'small' driver according to TSI [15The blue dashed line refers to the view line of both cases. The blue stars indicate the minimum and maximum distance from the driver to the front cabin window.

Table 2. Coordinates of the windshield control points for the longitudinal symmetry plane

Control point	x-coordinate	z-coordinate
$\mathbf{P}_3$	l_1	h_1
$\mathbf{P}_4$	$l_1 + k_2\min(l_2, s_2\cot\alpha_1)$	$h_1 - k_2\min(l_2\tan\alpha_1, s_2)$
$\mathbf{P}_5$	$l_1 + l_2$	h_2

Table 3. Range of variation of the design variables used for the geometric parameterization. Lengths are given in mm, while angles are in rad and parameters k are non-dimensional.

l_1	[700-2000]	h_3	[800-1300]	k_4	[0.30-0.80]	β_6	[0.00-0.10]	l_{loHO}	[350-500]
h_1	[3000-3600]	h_4	[250-500]	h_{WS}	[1500-1800]	$\boldsymbol{h_{HO}}$	[0.75-0.90]	$\boldsymbol{h_{loHO}}$	[150-300]
α_1	[0.16-0.52]	α_3	[0.26-0.87]	b_{WS}	[0.00-0.22]	$\boldsymbol{b_{HO}}$	[0.85-1.00]	$\boldsymbol{k_{Pico}}$	[0.85-1.00]
l_2	[1000-1500]	k_3	[0.20-0.80]	l_{upWS}	[0.80-1.00]	$\boldsymbol{l_{upHO}}$	[0.70-0.90]	$\boldsymbol{b_{Pico}}$	[800-1100]
h_2	[0.85-1.25]	l_4	[150-400]	h_{upWS}	[0.85-1.00]	$\boldsymbol{h_{upHO}}$	[0.85-1.00]	l_0	[0 - 1750]

METAMODEL DEFINITION

It has been indicated that the main drawback of the GA is the large number of evaluations required by the optimization method to find an optimal design. Each evaluation is usually a solver call, and the number of solver calls depends on the population size and the number of generations necessary to obtain the optimal design. This number of solver calls can be dramatically reduced if approximation models or metamodels are used with the GA. This is referred as surrogate-based optimization.

This number of evaluations is function of the number of individuals in the population and the number of generations necessary to obtain such optimal design. Apart from simplifying the geometric parameterization, the use of metamodels or approximation models permits By using approximation models, the expensive simulation model is replaced and so the GA process is speed up. The metamodel technique chosen in this paper is the radial basis function (RBF). It uses a linear combination of *m* radial basis functions

$$\hat{y}(\mathbf{x}) = \sum_{i=1}^{m} \omega_i \phi(|\mathbf{x} - \mathbf{x}_i|) \tag{4}$$

to approximate the response $\hat{y}(\mathbf{x})$. $\phi(d_i)$ is called the radial basis function, such that the radial distance d_i is defined as $d_i = |\mathbf{x} - \mathbf{x}_i|$ centered at the point $\mathbf{x}_i$. The norm || is the Euclidean distance. w_i is the weight of radial basis function *i* in the linear combination aforementioned. The radial function used here is the Gaussian function

$$\phi(d_i) = \exp\left(-\frac{d_i^2}{2|r_i|^2}\right) = \exp\left(-\frac{|x - x_i|^2}{2|r_i|^2}\right). \tag{5}$$

The construction of the RBF networks demands the estimation of some parameters. Apart from setting the weights in Eq. (4), the number of hidden units *m*, the spread *r* and the centers $\mathbf{x}_i$ are the other parameters to be defined. The number of neurons *m* is set equal to the size of the design of experiments *N* and the centers do coincide with the sampling points $\mathbf{x}_i$. The spread is fixed for all basis functions but varies for each design variable. The initial value is first estimated by the relation $r = d_{max}\sqrt{m}$, where d_{max} is the maximum distance between any two centers. Ridge regression is used to control the model sensitivity (avoid the model to overfit the data and to mislead variations due to imprecise or noisy data). A regularization parameter λ is introduced to the sum-squared-error expression applied to determine the optimal weight vector $w^m_{j=1}$. Orr proposes a parametric study to find the parameter λ and this strategy is also used in this paper. The model selection criteria used to find λ (and *r*) is the generalized cross-validation (GCV). Metamodel building involves choosing an 'experimental' design for generating a database and fitting the model to the observed data. The accuracy of the approximation predictions depends on the information contained in the database. To maximize this information

and fit the model by a representative sample of the design space Design of Experiments (DoE) method is applied. A 25-dimensional `maximin' Latin Hypercube design (LHD) of eighty points ($N \sim 3k$, where k is the dimensionality of the design space) is used to generate the DoE in MINAMO.

NUMERICAL SET-UP

Figure (3) shows the computational domain for this study. The inlet is placed $11H_t$ upstream the train head, the outlet is $20H_t$ far from the tail, and the lateral walls are $7H_t$ far from the train longitudinal symmetry plane. The top is $9H_t$ from the ground. The domain boundaries do not interfere with the flow around the vehicle and are in good agreement with the European normative, [15]. A constant velocity U_∞ of 50 ms^{-1} is used at the inlet of the computational domain. Uniform pressure is imposed at the outlet, and symmetry condition is set at the sides and top of the domain. The ground is moving with U_∞. The Reynolds number based on the inlet velocity and the train height is ~$1.3x10^7$. An incompressible, steady, turbulent flow simulation is considered. The k-ω SST turbulence model is used, with second order upwind momentum discretization scheme. The standard wall functions implemented in the CFD software are used at the ground and on the train surface. $y^+ = u_\tau y/\nu$, where u_τ is the wall friction velocity and ν is the kinematic viscosity of air, is fixed to 100. Δx^+ in terms of wall units y^+ is 25-250. A grid-independence analysis was performed.

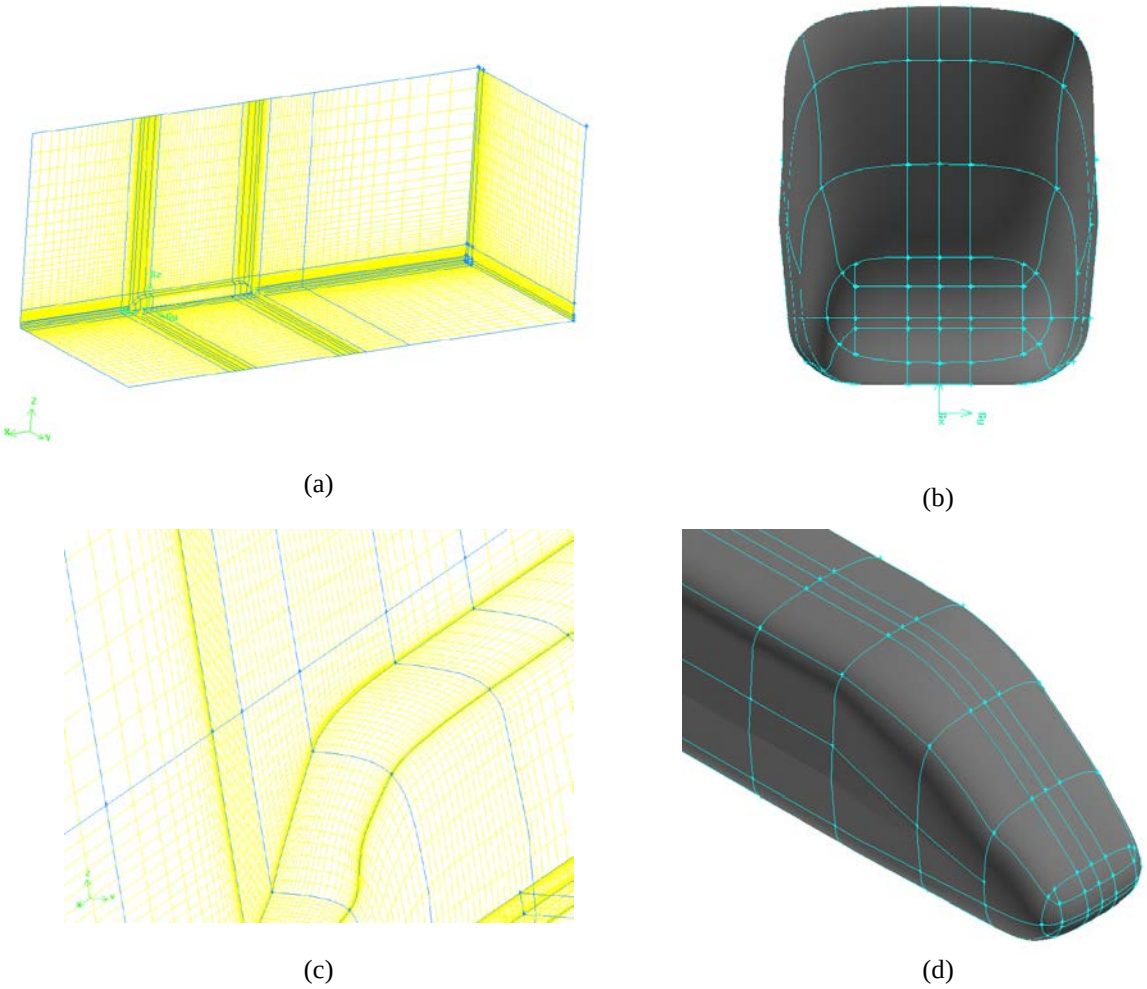

Fig. 3. (a) Computational domain and (c) detail of the boundary layer mesh along the train model; (b) and (d) refer to the original train (ATM).

DISCUSSION OF RESULTS

The values of the drag coefficient for the 80 geometries included in the initial DoE are indicated in Fig. (4a). The observed spread of the drag coefficient all along the initial data set shows the diversity of the geometries

englobed in the DoE. The mean value is 0.161, while the ATM geometry presents a drag coefficient of 0.166, what indicates that the reference geometry is very close to the mean performance of the design space. This confirms the choice of the range of the design variables. The best and worst design from the initial DoE are represented in Fig (4). Differences on the nose are evident. While geometry #21, which is the best design, is a slender nose, geometry #42 is a bluff nose, as it can be seen in Fig. (4c) and Fig (4d). More differences are observed in Fig (4a) and Fig (4b). Geometry #42 is shorter than#21, and the nose tip is elevated compared to the latter. This directly affects the stagnation point and all the pressure distribution on the front side of the train head. The nose shape of geometry #21 is quite similar to the well-known Spanish AVE duck-nose, although #21 presents a kind of bump around the hood that the actual AVE does not. Successive iterations are expected to remove this effect so that a smoother hood design might be obtained.

From this results and from the present metamodel, an optimization is run, resulting into two new designs. The optimization is run in MINAMO, being the most characteristic parameters of the optimization process those indicated in Table (3). It is important to remark that these new designs are given as one optimal design and one extra-point introduced to enhance the metamodel prediction in that regions of the design space where larger prediction error was observed. Nevertheless, when an accurate evaluation of the aerodynamic drag on these two designs is performed, it is obtained contradictory results. Indeed, geometry #81, which was supposed to be an optimal solution, gives a drag coefficient larger than the best design included in the initial DoE. This is explained because the prediction accuracy of the metamodel is still quite poor, and it needs to be re-trained.

A total number of 25 iterations are run after the initial DoE. It means 50 new geometries are analyzed in order to find the optimal design. The values of the design variables and the aerodynamic drag for these new designs are given in [16], while the evolution of the optimal solution at each iteration is presented in Fig. (5b). Squares are referred to these optimal designs at each new iteration, while crosses are related to extra-points introduced to improve the prediction capability of the metamodel. The spread of the latter indicates that points are added all along the design space although always far from the optimal region, as the drag coefficient is generally larger than the optimal one. On the other side, the convergence of the drag coefficient for the optimal solutions confirm that the GA has already detected the region where the optimal design is located. Small differences of the drag coefficient are observed for the last 10 iterations, so that it might be concluded that the optimization process has finished. In fact, if the best four designs of all the 130 geometries considered in the optimization are compared, it is possible to affirm that the optimal design has already been obtained. Figure (10) presents the lateral view of these four designs, and insignificant variations are observed between the nose shapes. The reference geometry (ATM or ICE2) is also represented in this figure. Not big differences are noticed around the nose tip, but the slope of the windshield and the hood has notably changed compared to the original one. The effect of these changes is more evident when the pressure field around the train nose and tail is studied. A reduction of about a 25% from the initial drag coefficient (0.166 of ATM to 0.122 of the best design) was obtained after validating the optimal candidates.

CONCLUSIONS

The tools considered for the optimization process, and also those for the metamodel building, permit a post-processing analysis, once the optimization is ended, to determine the influence of each design variable. It is also possible to study the prediction accuracy of the metamodel. Figures (5c) and (5d) show this precision in terms of the correlation coefficient (correlation between the actual value of the drag coefficient for the designs included in the DoE and predicted values by the metamodel). It is observed that the correlation coefficient is relatively low (0.65), but that after 50 iterations, this coefficient arises up to 0.75, value which still is larger when outliers are removed (0.81). This puts in evidence the capability of the metamodels, since the whole design space can be predicted with a precision of around 81%, being possible to give the exact value of the drag coefficient for train whose nose is defined with up to 25 design variables.

Figure (6a) shows the influence of each design variable on the drag coefficient. It is observed clearly that the most significant design variable is b_{Hood}, which is related to the width of the train nose (in particular at the hood cross-section). This result confirms the conclusions presented in previous studies, where the slenderness is vital for the reduction of the drag coefficient, [3]. A slender nose deflects the flow in such a way that the pressure distribution in the front face is lower. Variables l_1 and α_1 are related to the design of the roof and the nose length. These were also highlighted as critical variables in the comparison between geometries #21 and #42 and here it is again evident its role in the aerodynamic behavior of the train nose. l_2 is also a notable variable, being it related to the nose length. l_4, also denoted as k_4, and h_3 were mentioned as significant variables in the previous comparison. However, in Fig. (6a) it is observed that h_3 has not a so relevant role. This conclusion is taken since

there is no clear tendency of it to reduce the aerodynamic drag. Indeed, it is not h_3 by itself, but the combination of h_3 and k_4 that has a deeper impact on the deflection of the flow.

The correlation between the two most significant variables b_{Hood} an l_1, is shown in Fig. (6b). In order to reduce the aerodynamic drag , it is clear that it is necessary to decrease the value of b_{Hood}, what means a slenderer nose design. The larger l_1 is, the lower the drag coefficient is obtained.

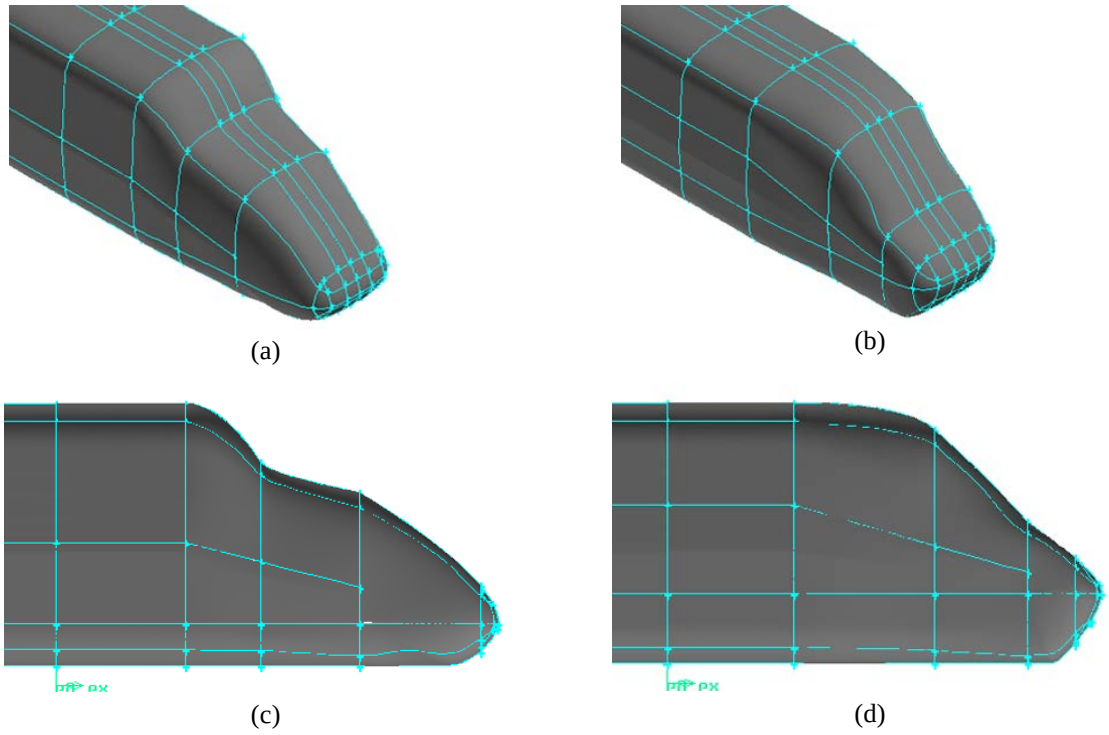

Fig. 4. Comparison of the best (#21) and worst (#42) geometry included in the initial DoE. (a) and (c) correspond to the 3D and the lateral view of geometry #21,while (b) and (d) to geometry #42.

However, the global minimum is not achieved with the largest value of l_1. In fact, a decrease of l_1 provokes an increase of the nose length. If l_1 is too short, the nose slant angle is too large, leading to the detachment of the flow. As l_1 increases, the transition point between the train head and the train body is closer to the nose tip (in other words, the train head length decreases). According to the present geometry parameterization, such evolution lets reduce the slant angle. However, a further increase of l_1 would notably decrease the train head length, and so increase the flow detachment.
The evolution of some of the most significant variables are shown in Fig. (7a) to (7e). The convergence of these is observed in the plots. It is important to remark that the dispersion of the values of the design variables is due to the fact that at each iteration, an optimal candidate and an extra point to improve the prediction accuracy of the metamodel are introduced. Therefore, if just the values of the design variables for the optimal candidates are considered, such convergence is appreciated.

To complete the analysis of the influence of each design variable on the total aerodynamic drag, and in order to show more clearly the comparison of the initial and the optimal design (#130), in Fig. (8) the pressure field at the train head and at the symmetry plane are represented. Furthermore, the pathlines at the train tail are also depicted to show the differences of the vortices created at the rear part of the train. It is evident the different nature of these vortices for the original case Fig. (9a) and for the optimal one Fig. (9b).

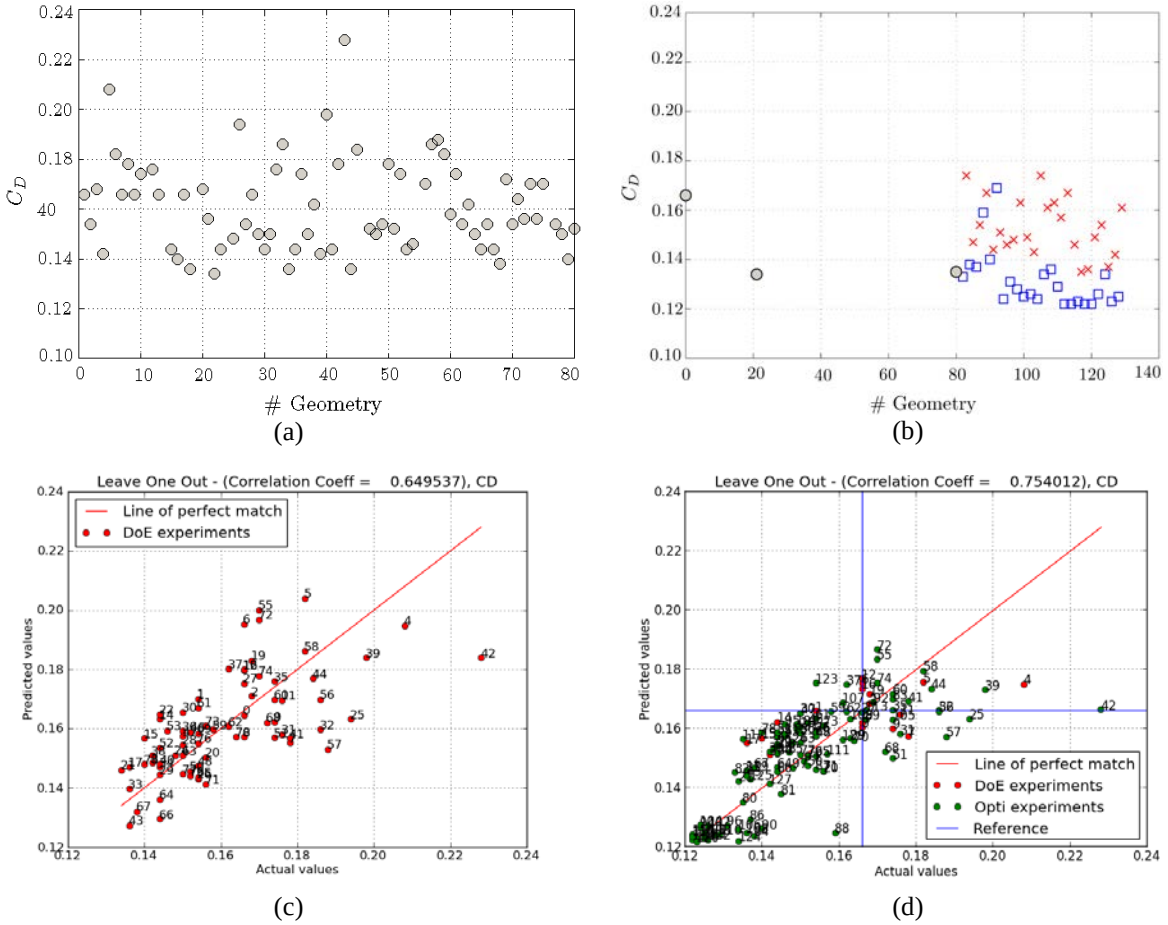

Fig. 4. (a) Drag coefficient values for the 80 cases of the initial DoE; (b) Evolution of the drag coefficient C_D along the optimization process; (c) Correlation coefficient for the metamodel at the initial DoE and (d) after 25 iterations.

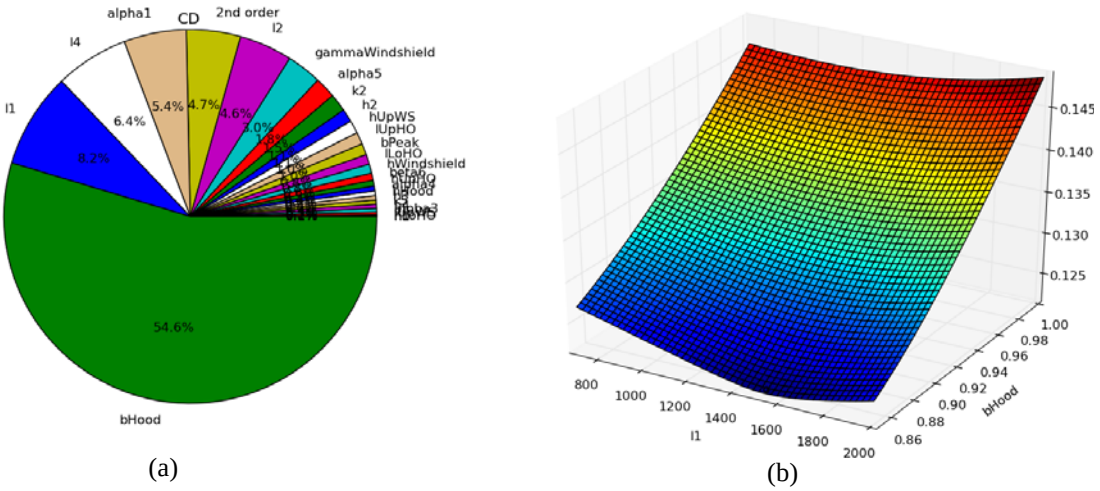

Fig. 5. (a) ANOVA test. (b) Correlation between b_{Hood} and l_1 with the drag coefficient.

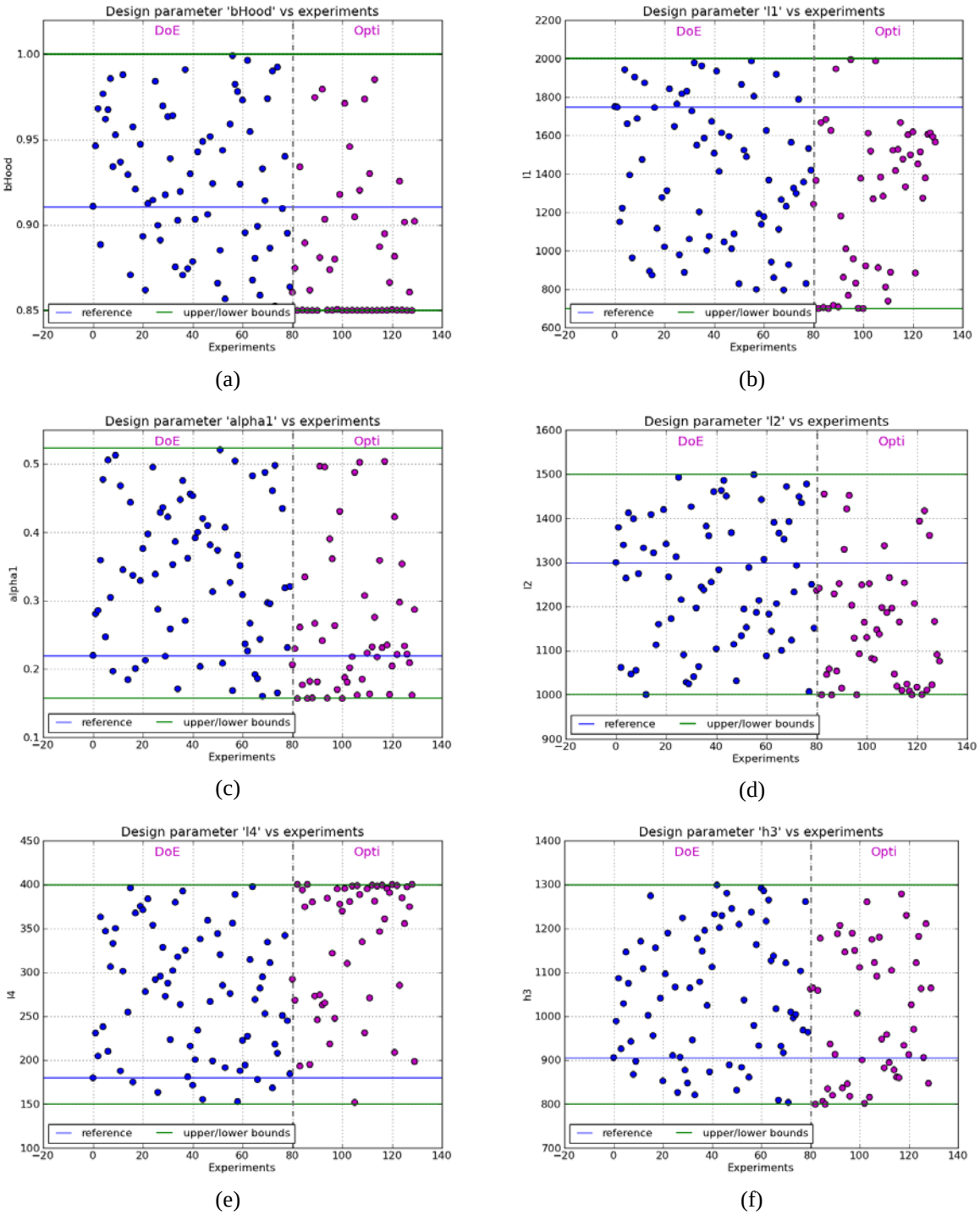

Fig. 7. Evolution of a) b_{Hood}; (b) l_1; (c) α_1; (d) l_2; (e) l_4 and (f) h_3 along the optimization process.

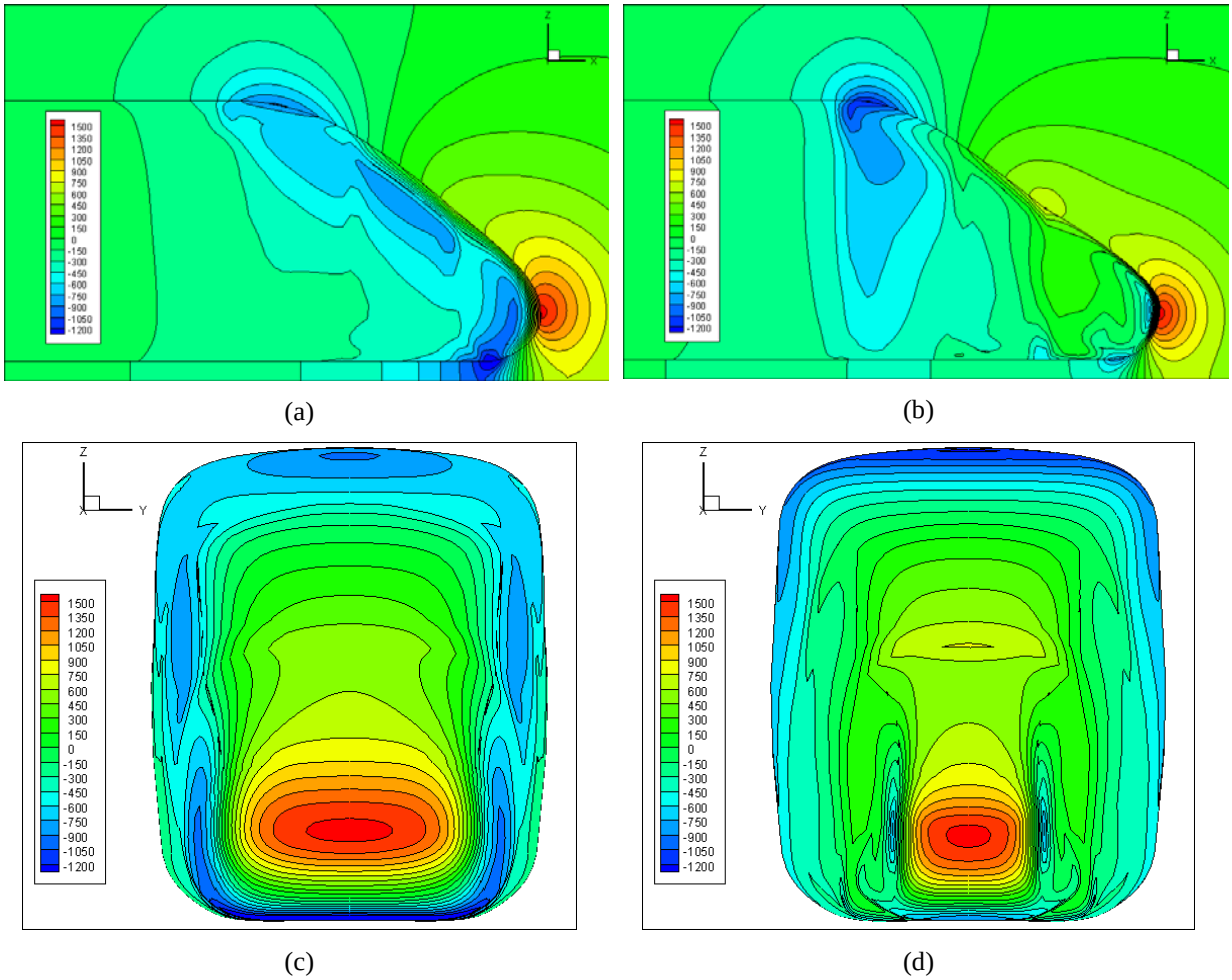

(a) (b)

(c) (d)

Fig. 8. Pressure field at the train nose and the symmetry plane for (a) and (c) #1 (ATM train model); and for (b) and (d) the optimal design (#130).

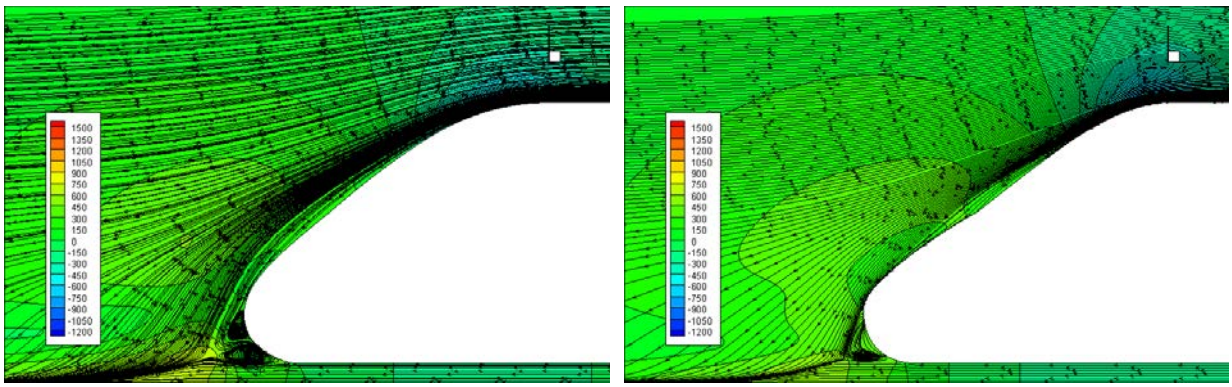

(a) (b)

Fig. 9. Pathlines at the train tail for (a) #1 (ATM train model) and (b) for the optimal design (#130).

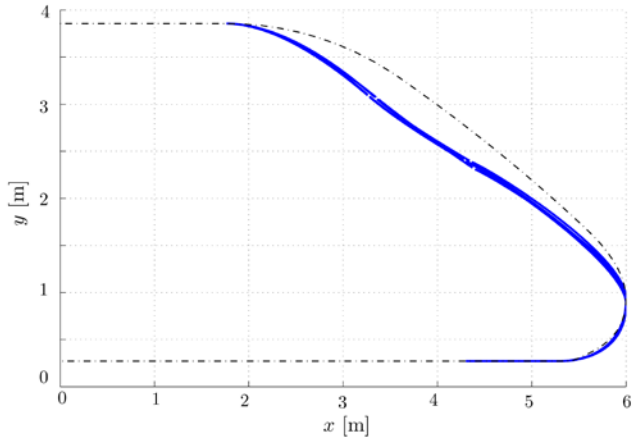

Fig. 10. Lateral view of the best four designs obtained in the optimization process for its comparison with the initial shape of ATM train model.

ACKNOWLEDGMENTS

This work is financed by Ministerio de Ciencia e Investigación under contract TRA-2010-20582, included in the VI Plan Nacional I+D+i 2008-2011.

REFERENCE

[1] C. Baker, *The Flow Around High Speed Trains*, BBAA VI International Colloquium on Bluff Bodies Aerodynamics & Applications, Milano, Italy (2008).
[2] H. Choi, J. Lee, H. Park, *Aerodynamics of Heavy Vehicles*, Ann. Rev. Fluid Mech., 46 (2014), 441-468.
[3] R. S. Raghunathan, H. -D. Kim, T. Setoguchi, *Aerodynamics of High-Speed Railway Train*, Progress in Aerospace Sciences 38 (2002), 469-514.
[4] J. A. Schetz, *Aerodynamics of High-Speed Trains*, Ann. Rev. Fluid Mech., 33 (2001), 371-414.
[5] H. Sockel, *Handbook of Fluid Dynamics and Fluid Machinery*, chapter The aerodynamics of trains, Wiley and Sons (1996).
[6] A. Orellano, M. Schober, *Aerodynamic Performance of a Typical High-Speed Train*. In 4th WSEAS International Conference on Fluid Mechanics and Aerodynamics, Elounda, Greece (2006).
[7] J. Osth, S. Krajnovic, *A Study of the Aerodynamics of a Generic Container Freight Wagon using Large-Eddy Simulation*, J. Wind Eng. Ind. Aero., 44 (2014), 31-51.
[8] F. Cheli, D. Rocchi, F. Ripamonti, G. Tomasini, *Aerodynamic Behaviour Investigation of the new EMUV 250 Train to Cross-wind*, J. Wind Eng. Ind. Aero. 98 (2010), 189-201.
[9] A. Orellano, *Aeroefficient - optimized train*. In modeFRONTIER International Users Meeting 2010, Trieste, Italy (2010).
[10] J. Muñoz-Paniagua, J. García, A. Crespo, Genetically Aerodynamic Optimization of the Nose Shape of a High-Speed Train entering a Tunnel, J. Wind Eng. Ind. Aero. 130 (2014), 48-61.
[11] S. Krajnovic, Optimization of Aerodynamic Properties of High-Speed Trains with CFD and Response Surface Models. In *The Aerodynamics of Heavy Vehicles II*: Trucks, Buses and Trains, Springer (2009).
[12] J. H. Holland, *Adaptation in Natural and Artificial Systems*. The University of Michinga Press (1975).
[13] D.E.Goldberg, Genetic Algorithms in Search, Optimization and Machine Learning, Addison-Wesley (1989).
[14] ANSYS Inc. *ANSYS FLUENT Adjoint Solver. Release 14.5*, (2012).
[15] EN 14067-4:2005+A1. Railway Applications - Aerodynamics. Part 4. (2009).
[16] J. Muñoz-Paniagua, Aerodynamic Optimization of the Nose Shape of a High-Speed Train, Univ. Politécnica de Madrid (2014).